RSC Advances

PAPER

Check for updates

A long-persistent phosphorescent chemosensor for the detection of TNP based on CaTiO₃:Pr³⁺@SiO₂ photoluminescence materials†

Fangfang Li,[a] Fengyi Wang,[a] Xuan Hu,[a] Baozhan Zheng,[a] Juan Du (ID) *[ab] and Dan Xiao (ID) *[ab]

The detection of nitroaromatic explosives is important due to their strong explosive force and harmfulness in the environment, and for homeland security and public safety. Herein, a phosphorescence CaTiO₃:Pr³⁺@SiO₂ nanosensor was successfully developed for the sensitive and selective detection of 2,4,6-trinitrophenol (TNP). The red-emitting phosphorescent chemosensor CaTiO₃:Pr³⁺@SiO₂ possessed a long enough phosphorescence lifetime of 0.016 s. The TNP induced phosphorescence quenching process of CaTiO₃:Pr³⁺@SiO₂ presented a wide linearity with TNP concentrations ranging from 0.5 to 100 μM, and the detection limit was found to be 20.6 nM. Furthermore, this sensor displayed a high selectivity toward TNP over other structurally similar compounds like 2,4,6-trinitrotoluene (TNT), 2,4-dinitrotoluene (DNT), 4-nitrotoluene (NT), 2,4-dinitrophenol (DNP), 4-nitrophenol (NP) and phenol. This sensing system was successfully used in the test of TNP concentrations in water samples, and showed great potential for practical application.

Introduction

2,4,6-Trinitrophenol (TNP), known as picric acid, is a common reagent widely used in the in the preparation of matches, fireworks, explosives, fungicides, glasses, rocket fuels, chemical fibers and dyes.[1–4] Compared to other nitroaromatic compounds such as 2,4,6-trinitromethylbenzene (TNT) and 2,4-dinitrotoluene (DNT), TNP has stronger explosive power and higher thermal-expansion.[5,6] It needs to be noted that due to the high solubility of TNP in water, it can easily contaminate soil and groundwater and accumulate in natural waters over the long-term during its testing, usage, storage, and dumping.[7–12] Once TNP enters the human body, it will cause harm such as neurological disorders, convulsions, abdominal pain, headache, dizziness, and even cancer.[13,14] Therefore, selective and sensitive detection of TNP has attracted increasing attention in view of homeland security and personal safety.

Currently, different techniques have been developed for the determination of TNP, including infrared and Raman spectroscopy,[15] high-pressure liquid chromatography,[16] mass spectrometry,[17,18] surface-enhanced Raman spectroscopy,[19] colorimetric[1] and electrochemical.[20] Unfortunately, most of these methods are complicated or time-consuming, and involve complex operation of expensive instruments, all of which will impede their widespread application. Photoluminescence (PL)-based chemosensors have gained more attention because of their low instrumentation cost, short response time, high sensitivity and selectivity.[21,22] On the other hand, when using an optical sensing technology, a large background fluorescence signal will cause a negative impact during detection process,[23,24] Compared with fluorescent materials, phosphorescent materials can eliminate the interference from short-lived fluorescent background by using time-resolved technology, with added advantages of high luminescence efficiency, and good photo and thermal stabilities.[25–27] Nevertheless, so far there are few reports about detecting nitroaromatic explosives by means of phosphorescence method.

In recent years, the photoluminescence materials of alkaline earth titanates doped with rare earth ions have attracted research interests due to their high chemical stability.[28] Most titanates photoluminescence materials were widely used in the fields of emergency lighting, interior decoration, road signs and AC-LEDs.[29–31] Among which, CaTiO₃:Pr³⁺ photoluminescence materials became very popular due to its persistent afterglow phenomenon. CaTiO₃:Pr³⁺ material has perovskite structure, when Pr³⁺ incorporates in CaTiO₃ perovskite, it yields a single red emission, from the $^1D_2$–$^3H_4$ transition, due to the overlying inter-valence charge transfer that completely depopulates the $^3P_0$ state.[32,33] Recently, CaTiO₃:Pr³⁺ material has received more attention because of its good persistent characteristics with chromaticity coordinate close to the "ideal red", excellent

[a]College of Chemistry, Sichuan University, 29 Wangjiang Road, Chengdu 610064, China. E-mail: dujuanchem@scu.edu.cn; xiaodan@scu.edu.cn

[b]Key Laboratory of Green Chemistry and Technology, Ministry of Education, College of Chemistry, Sichuan University, Chengdu 610064, China

chemical/physical stability, and eco-friendliness.[34,35] In order to gain a better performance, great efforts have been made to prepare the nano-sized CaTiO$_3$:Pr^{3+} photoluminescence material, such as solid-state reaction,[36] precipitation technique,[37] sol–gel process[38] and hydrothermal synthesis.[39] As a persistent phosphorescent material, CaTiO$_3$:Pr^{3+} has attracted considerable attention for various displays and signing applications in dark environments. However, until now, there were no attention to the determination of nitroaromatic explosives using CaTiO$_3$:Pr^{3+}.

In the present work, we prepared long-persistent red-emitting CaTiO$_3$:Pr^{3+} photoluminescence material under solid-state synthesis method. Because of its poor solubility in many solvents, the CaTiO$_3$:Pr^{3+} nanoparticles should be functionalized to make it solvent-stable before utilization as a photoluminescence probe. Herein, the CaTiO$_3$:Pr^{3+} nanoparticles can be uniformly dispersed in water *via* a facile strategy of coating a silica shell on the CaTiO$_3$:Pr^{3+} surface to form a photoluminescence composite material, and presented an example of application of CaTiO$_3$:Pr^{3+}@SiO$_2$ nanoparticles for TNP detection. In this work, CaTiO$_3$:Pr^{3+}@SiO$_2$ nanoparticles displayed a high sensitivity toward TNP over other structurally similar compounds like 2,4,6-trinitrotoluene (TNT), 2,4-dinitrotoluene (DNT), 4-nitrotoluene (NT), 2,4-dinitrophenol (DNP), 4-nitrophenol (NP) and phenol. This assay can effectively detect TNP range from 0.5 μM to 100 μM with a detection limit of 20.6 nM. This method was also successfully used to analyze TNP in natural water samples.

Experimental section

Chemicals

Praseodymium oxide (Pr$_6$O$_{11}$), 2,4,6-trinitrophenol (TNP), 2,4,6-trinitrotoluene (TNT), 2,4-dinitrotoluene (DNT), 4-nitrotoluene (NT), 2,4-dinitrophenol (DNP), 4-nitrophenol (NP) and phenol were purchased from Aladdin (Shanghai, China); orthoboric acid (H$_3$BO$_3$), titanium oxide (TiO$_2$), calcium nitrate tetrahydrate (Ca(NO$_3$)$_2$·4H$_2$O) were purchased from Chengdu Chemical Reagent Company (Chengdu, China); tetraethyl orthosilicate (TEOS), cyclohexane, *n*-hexanol, and Triton X-100 (TX-100) were purchased from Tianjin Reagent Plant (Tianjin, China). All the other chemicals were of analytical-reagent grade and used without further purification.

Apparatus

UV-visible spectra were measured on Hitachi U-2900 spectrophotometer equipped with a 1 cm quartz cell. Phosphorescence spectra were measured on Hitachi F-7000 spectrophotometer equipped with a 1 cm quartz cell. Scanning electron microscopy (SEM) images were recorded on a field emission Hitachi S4800 microscope (Japan) equipped with a Oxford energy-dispersive X-ray (EDX) detector (UK) to perform the elemental mapping. X-ray diffraction (XRD) measurement was acquired on a Tongda TD-3500 X-ray powder diffractometer (Liaoning, China) with Cu Kα radiation. Phosphorescence lifetime was measured on a Fluorolog-3 spectrofluorometer (Horiba JobinYvon) with

a Spectra LED (280 nm, S-280, Horiba Scientific) as the excitation source and a picosecond photon detection module (PPD-850, Horiba Scientific) as the detector. The Particle size were measured on a Malvern Nano ZS90 Zetasizer Nano instrument (Worcestershire, UK).

Preparation of the CaTiO$_3$:Pr^{3+} nanoparticles

CaTiO$_3$:Pr^{3+} were prepared by a solid-state synthesis method as described in the literature with a little modification.[40] Pr^{3+} was introduced in the form of Pr(NO$_3$)$_3$ by dissolving Pr$_6$O$_{11}$ into HNO$_3$. Ca(NO$_3$)$_2$·4H$_2$O, TiO$_2$, and Pr^{3+} were weighed according to the nominal compositions of CaTiO$_3$:xPr^{3+} (x = 0%, 0.1%, 0.4% and 1%), and 3 wt% H$_3$BO$_3$ was added as a flux, then they were mixed by ultrasonic cleaner at room temperature for 15 min, the mixture was put into tube furnace to sinter at 900 °C for 1–5 h. At last, white powder samples CaTiO$_3$:Pr^{3+} were gained.

Synthesis of CaTiO$_3$:Pr^{3+}@SiO$_2$ nanoparticles

Typically, 15 mL cyclohexane, 3.4 mL Triton X-100 and 3.6 mL 1-hexanol are mixed uniformly, after stirring for 5 minutes, a certain concentration of as-prepared CaTiO$_3$:Pr^{3+} nanoparticles (50 mg) and 300 μL deionized water were added to a beaker under stirring to form a w/o microemulsion. Then 100 μL tetraethyl orthosilicate (TEOS) and 100 μL ammonia aqueous solution were added to the microemulsion and the sample was mechanically stirred for 24 h at room temperature. To separate the particles, ethanol was added to break the microemulsion. The resulting nanocomposites were centrifuged and washed repeatedly with water and ethanol and then dried in vacuum at 40 °C overnight.

Results and discussion

Preparation and characterization of CaTiO$_3$:Pr^{3+}@SiO$_2$ nanoparticles

As mentioned previously, the strong phosphorescence CaTiO$_3$:Pr^{3+} nanoparticles were prepared by solid phase method. We tested the phosphorescence intensity of CaTiO$_3$:Pr^{3+} with different mole ratios of Pr^{3+} and calcination time. Fig. S1† exhibited the phosphorescence spectra of CaTiO$_3$:xPr^{3+} (x = 0–1%) samples upon 315 nm excitation. The sample had no phosphorescence emission intensity at x = 0, and the

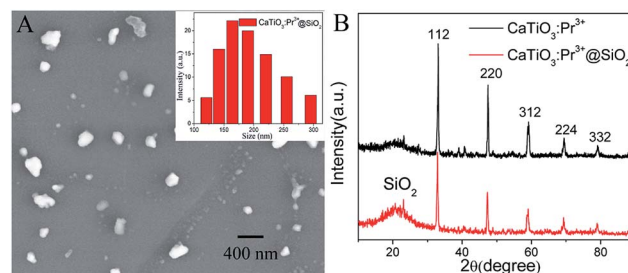**Fig. 1** (A) SEM image of CaTiO$_3$:Pr^{3+}@SiO$_2$ nanoparticles, (inset: size distribution of CaTiO$_3$:Pr^{3+}@SiO$_2$ nanoparticles), (B) XRD pattern of CaTiO$_3$:Pr^{3+} and CaTiO$_3$:Pr^{3+}@SiO$_2$ samples.

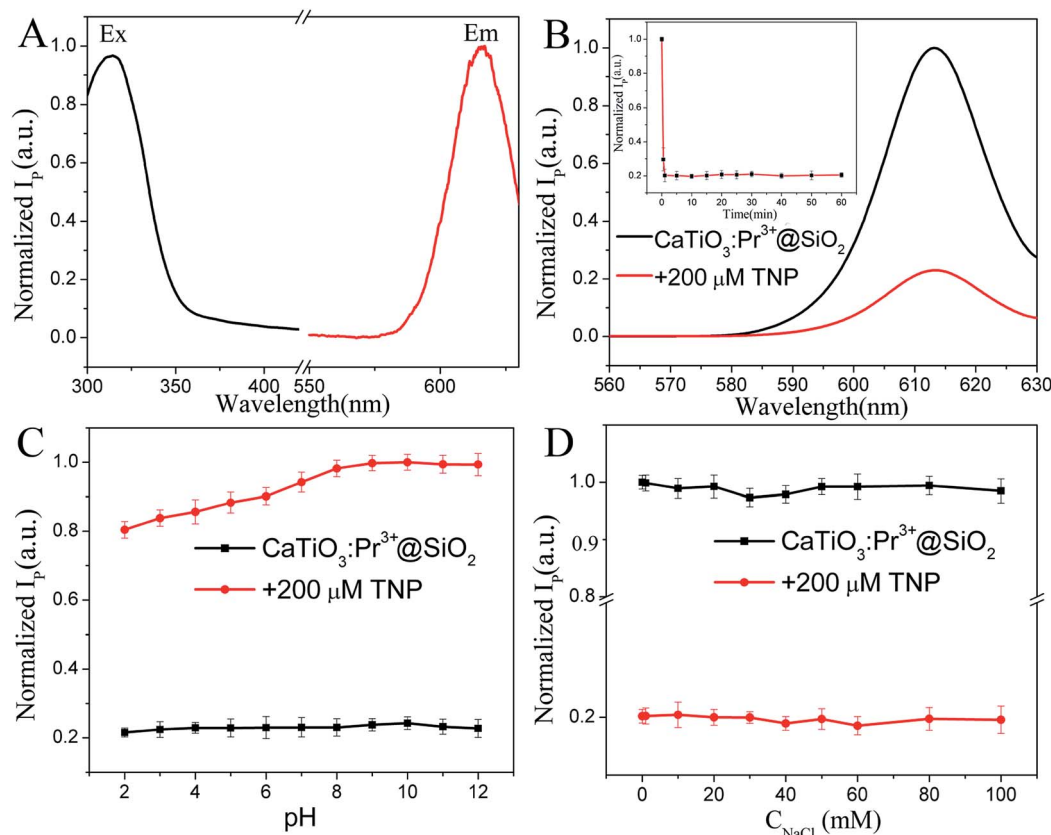**Fig. 2** (A) Phosphorescence excitation (Ex) and emission spectra (Em) of $CaTiO_3$:Pr^{3+}@SiO_2 (30 μg mL^{-1}) in PBS solution (10 mM, pH = 8.0), (λ_{Ex} = 315 nm, λ_{Em} = 614 nm). (B) Phosphorescence spectra of 30 μg mL^{-1} $CaTiO_3$:Pr^{3+}@SiO_2 with (red curve) and without (black curve) 200 μM TNP. Inset: temporal change in the phosphorescence intensity of $CaTiO_3$:Pr^{3+}@SiO_2 after the addition of TNP. Effect of (C) pH and (D) salt concentration on the phosphorescence intensity of $CaTiO_3$:Pr^{3+}@SiO_2 (30 μg mL^{-1}) in the absence (black line) and presence (red line) of 200 μM TNP. λ_{Ex} = 315 nm (error bars, SD, n = 3).

phosphorescence intensity of $CaTiO_3$:Pr^{3+} nanoparticles at x = 0.4% was the highest in those red phosphorescence materials with different mole ratios of Pr^{3+}. The sample sintered at 900 °C for 3 h showed the maximum phosphorescence intensity in Fig. S1B.† Here, the samples used in the later measurements were prepared at Pr^{3+} mole ratio 0.4%, calcination temperature 900 °C and calcination time 3 h. We also investigated the phosphorescence behavior of $CaTiO_3$:Pr^{3+} before and after coated a silica shell. The phosphorescence intensity of $CaTiO_3$:Pr^{3+} decreased after coated a silica shell (Fig. S2A†), but the phosphorescence intensity of $CaTiO_3$:Pr^{3+}@SiO_2 hardly changed within 2 h under 315 nm excitation. Compared with the ~30% decrease in phosphorescence intensity of $CaTiO_3$:Pr^{3+} in about 2 h (Fig. S2B†), it can be inferred that the $CaTiO_3$:Pr^{3+}@SiO_2 nanoparticles had better photo-stability than $CaTiO_3$:Pr^{3+}. $CaTiO_3$:Pr^{3+}@SiO_2 nanoparticles were used in later experiments.

The micromorphology analysis of $CaTiO_3$:Pr^{3+}@SiO_2 nanoparticles were carried out using scanning electron microscopy (SEM). As showed in Fig. 1A, $CaTiO_3$:Pr^{3+}@SiO_2 nanoparticles were uniformly dispersed with diameters of 115–300 nm, and the average size was 201 nm (inset of Fig. 1A). Fig. 1B showed the diffraction peak positions and the relative intensities of

$CaTiO_3$:Pr^{3+} and $CaTiO_3$:Pr^{3+}@SiO_2, respectively. The discernible five diffraction peaks could be indexed to (112), (220), (312), (224) and (332), which matched well with the database of perovskite in JCPDS (JCPDS Card no. 01-081-0561) file. The same position of characteristic peaks for $CaTiO_3$:Pr^{3+} and $CaTiO_3$:Pr^{3+}@SiO_2 indicated the stability of the crystalline phase of $CaTiO_3$:Pr^{3+} nanoparticles during silica coating. Besides the peak of $CaTiO_3$, the XRD pattern of $CaTiO_3$:Pr^{3+}@SiO_2 (red line) presented abroad XRD peak at low diffraction angle ~21°, which attributed to the amorphous state SiO_2 shells. Moreover, EDS elemental mapping images presented in Fig. S3† verify the presence of O, Si, Ca and Ti elements in $CaTiO_3$:Pr^{3+}@SiO_2.

Phosphorescence sensing to TNP

Upon 315 nm excitation, a very intense single red emission band at 614 nm was found in the phosphorescence spectrum of $CaTiO_3$:Pr^{3+}@SiO_2 (Fig. 2A), corresponding to the characteristic $^1D_2 \rightarrow {}^3H_4$ transition of Pr^{3+}.[28] The phosphorescence intensity was significantly quenched by ~80% with the addition of 200 μM TNP (Fig. 2B). The response time for $CaTiO_3$:Pr^{3+}@SiO_2 toward TNP was within 1 min (the inset of Fig. 2B).

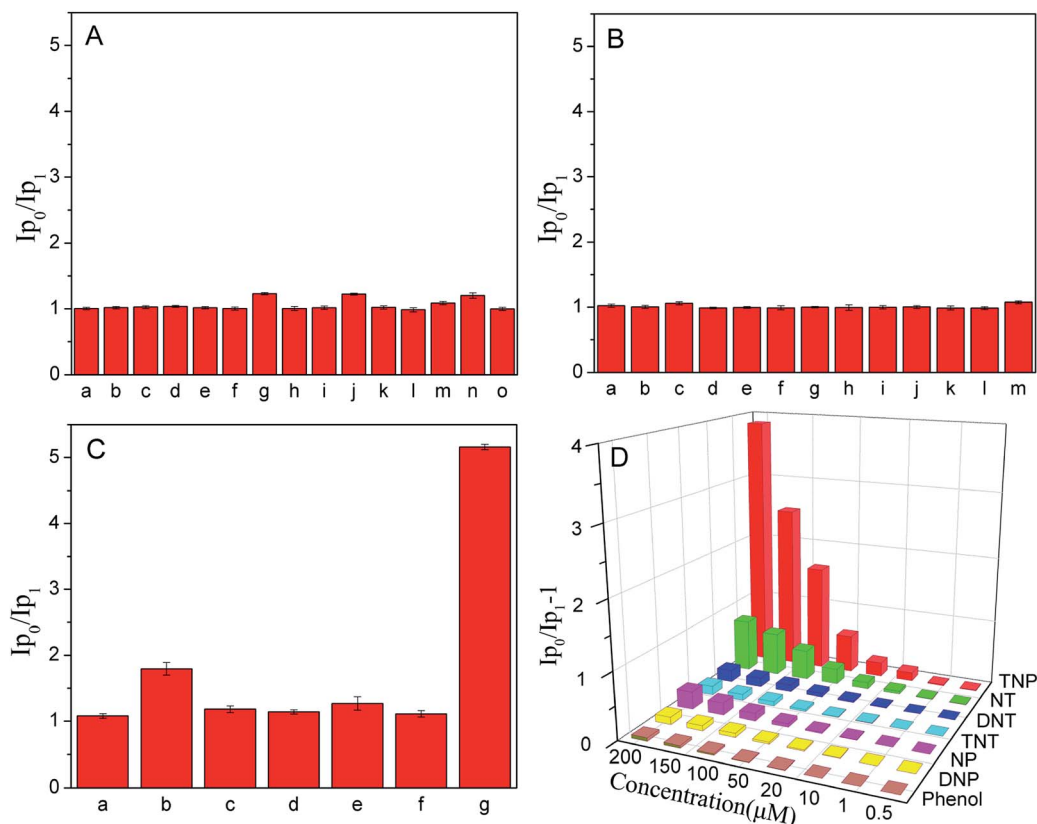**Fig. 3** (A–C) Relative phosphorescence intensities (Ip_0/Ip_1) of $CaTiO_3:Pr^{3+}@SiO_2$ (30 μg mL^{-1}) to 200 μM possible interfering substance in PBS solution (10 mM, pH = 8.0). (A): (a) Na^+, (b) Mg^{2+}, (c) Al^{3+}, (d) Ca^{2+}, (e) Cr^{3+}, (f) Mn^{2+}, (g) Fe^{3+}, (h) Co^{2+}, (i) Ni^{2+}, (j) Cu^{2+}, (k) Zn^{2+}, (l) Cd^{2+}, (m) Ag^+, (n) Hg^{2+}, (o) Pb^{2+}. (B): (a) F^-, (b) Cl^-, (c) Br^-, (d) I^-, (e) CO_3^{2-}, (f) oxalate, (g) citrate, (h) NO_3^-, (i) NO_2^-, (g) SO_4^{2-}, (k) SO_3^{2-}, (l) S^{2-}, (m) PO_4^{3-}. (C): (a) Phenol, (b) NT, (c) DNT, (d) TNT, (e) NP, (f) DNP, (g) TNP. (D): Phosphorescence quenching efficiencies ((Ip_0/Ip_1) − 1) obtained from different nitroaromatic explosives. Where Ip_1 and Ip_0 were the phosphorescence intensity of $CaTiO_3:Pr^{3+}@SiO_2$ with and without these possible interfering substance. λ_{Ex} = 315 nm (error bars, SD, n = 3).

The phosphorescence behavior of $CaTiO_3:Pr^{3+}@SiO_2$ in absence and presence of 200 μM TNP in various PBS buffer at pH 2–12 were measured (Fig. 2C). The phosphorescence intensity of $CaTiO_3:Pr^{3+}@SiO_2$ in the absence of TNP was slowly raised in the pH range from 2 to 8, and was comparatively stable when pH > 8. The phosphorescence intensity of $CaTiO_3:Pr^{3+}@SiO_2$ was comparatively stable in the presence of TNP in the whole pH range from 2 to 12. Considering the more stable phosphorescence intensity of $CaTiO_3:Pr^{3+}@SiO_2$ without TNP in the in the pH range from 8 to 12, a weak alkaline condition of pH 8.0 (PBS, 10 mM) was used for the later phosphorescence measurements.

The phosphorescence intensity of $CaTiO_3:Pr^{3+}@SiO_2$ in the absence and presence of 200 μM TNP remained almost constant when exposed to 0–100 mM NaCl solution (Fig. 2D), indicating that ionic strength just had negligible effect on the detection of TNP. The dramatic phosphorescence intensity decrease, short response time and stable phosphorescence behavior in wide pH range and high ionic strength demonstrated the great potential of $CaTiO_3:Pr^{3+}@SiO_2$ nanoparticles as effective TNP probe.

Specificity of $CaTiO_3:Pr^{3+}@SiO_2$ toward TNP

To verify the specific recognition of $CaTiO_3:Pr^{3+}@SiO_2$ to TNP, we investigated the phosphorescence behavior of $CaTiO_3:Pr^{3+}@SiO_2$ to different metal ions (200 μM), anions (200 μM) and nitroaromatic explosives (200 μM) in PBS(10 mM, pH 8.0). As showed in Fig. 3, the phosphorescence intensity of $CaTiO_3:Pr^{3+}@SiO_2$ had no obvious change in the presence of the above mentioned substances except that only several nitroaromatic explosives induced a negligible phosphorescence intensity decrease. The quenching efficiency for various

Table 1 Phosphorescence quenching constant (K_{S-V}) values for different nitro explosives

Analytes	K_{S-V} values ($\times 10^4$)	Correlation coefficient (R^2)
TNP	1.25	0.999
NT	0.41	0.992
DNT	0.090	0.991
TNT	0.067	0.995
NP	0.13	0.993
DNP	0.053	0.994
Phenol	0.025	0.995
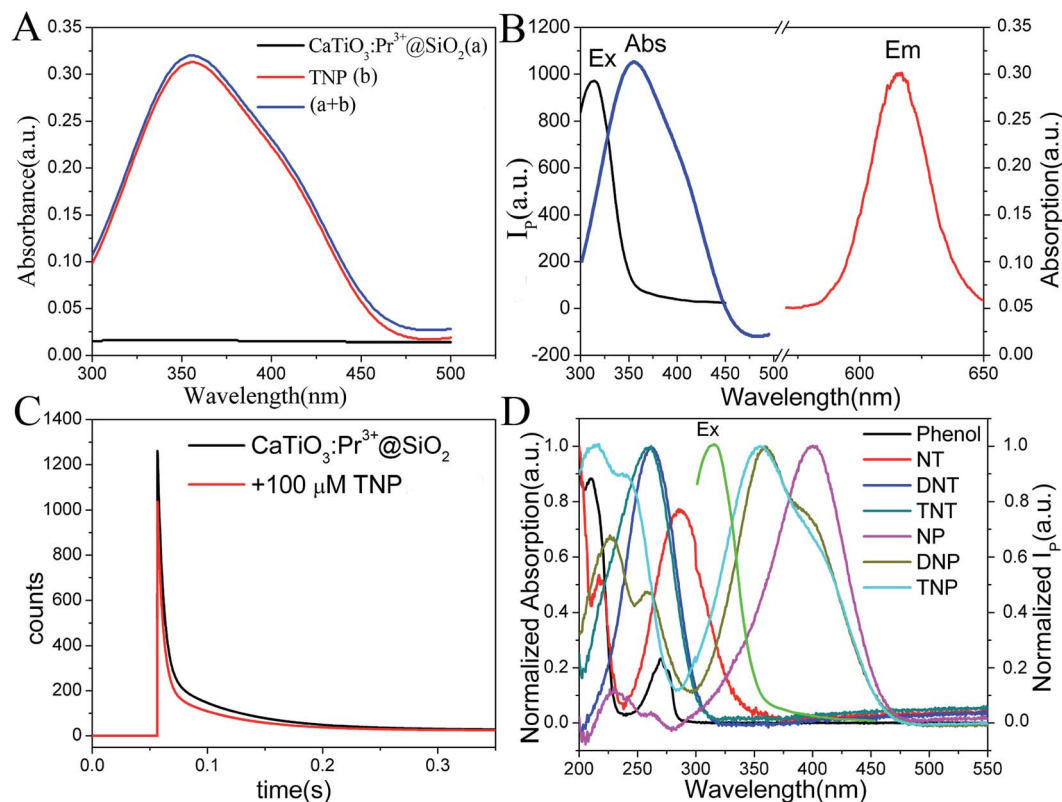
Fig. 4 (A) UV-vis absorption spectra of CaTiO$_3$:Pr^{3+}@SiO$_2$ and TNP, and the sum of CaTiO$_3$:Pr^{3+}@SiO$_2$ and TNP. (B) UV-vis absorption spectrum of TNP and the phosphorescence excitation and emission spectra of CaTiO$_3$:Pr^{3+}@SiO$_2$. (C) Time-resolved decay of CaTiO$_3$:Pr^{3+}@SiO$_2$ with and without 100 μM TNP. (D) Spectral overlap between excitation spectrum of CaTiO$_3$:Pr^{3+}@SiO$_2$ and absorption spectra of different nitroexplosive compounds in PBS solution (10 mM, pH = 8.0).

nitroaromatic explosives (2,4,6-trinitrotoluene (TNT), 2,4-dinitrotoluene (DNT), 2-nitrotoluene (NT), 2,4-dinitrophenol (DNP), 4-nitrophenol (NP) and phenol) was also estimated by using the Stern–Volmer (SV) equation,

$$I_0/I = 1 + K_{SV}[Q]$$

where I_0 and I are phosphorescence intensities in the absence and presence of nitro explosive, $[Q]$ is the molar concentration of analytes and K_{SV} is the quenching constant (M^{-1}). The quenching constants were shown in Table 1. The K_{SV} of TNP was found to be 1.25×10^4 M^{-1}, which was much larger than other nitro aromatics, suggesting the predominant selectivity of CaTiO$_3$:Pr^{3+}@SiO$_2$ toward TNP. Another important feature of CaTiO$_3$:Pr^{3+}@SiO$_2$ was its high selectivity toward TNP in a competitive environment. The competitive experiments were conducted in the presence of TNP and various other metal ions, anions and nitroaromatic explosives. The results shown in Fig. S4† displayed that there were no distinct variations of the phosphorescence signal caused by the coexistence of these species.

Investigation of the detection mechanism

In order to probe the origin of the high selectivity of CaTiO$_3$:Pr^{3+}@SiO$_2$ toward TNP, the quenching process was studied. In general, as shown in Fig. 4A, the UV-vis absorption spectrum of the sum of CaTiO$_3$:Pr^{3+}@SiO$_2$ and TNP was very similar to that of TNP alone except a slight difference in the intensity. This phenomenon indicated that the no Meisenheimer complexes between CaTiO$_3$:Pr^{3+}@SiO$_2$ and TNP were formed.[41] As shown in Fig. S5 in the ESI,† no new absorption peak but increased absorption intensity could be observed with the increasing concentration of TNP. These results excluded the possibility of a charge-transfer mechanism between TNP and CaTiO$_3$:Pr^{3+}@SiO$_2$. As displayed in Fig. 4C, the photoluminescence lifetime of CaTiO$_3$:Pr^{3+}@SiO$_2$ in the absence and presence of 100 μM TNP remained nearly constant, and the phosphorescence decay was fitted using a two-exponential decay function to yield a lifetime of 0.016 s. The unchanged lifetime excluded the possibility of the FRET process between CaTiO$_3$:Pr^{3+}@SiO$_2$ and TNP. Fig. 4B showed the excitation spectrum and emission spectrum of CaTiO$_3$:Pr^{3+}@SiO$_2$ and the absorption spectrum of TNP. An obvious overlap between the excitation spectrum of CaTiO$_3$:Pr^{3+}@SiO$_2$ and the absorption spectrum of TNP can be noticed. Owing to the strong absorption of TNP, the excitation light for CaTiO$_3$:Pr^{3+}@SiO$_2$ was weakened by an inner filter effect (IFE) process. Therefore, the IFE could be considered as one major process in the phosphorescence quenching behavior of the CaTiO$_3$:Pr^{3+}@SiO$_2$ after addition of TNP. As comparison, there were little overlap between the UV-vis absorption spectra
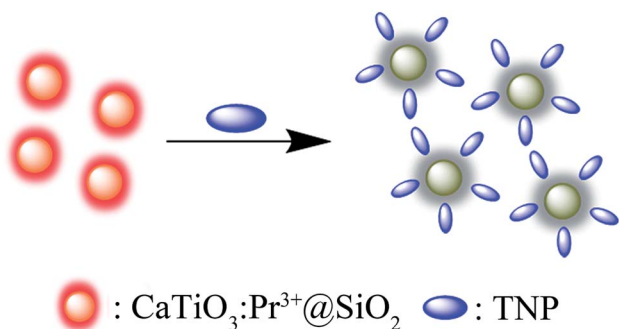
Scheme 1 Scheme for the phosphorescence quenching detection of TNP based on the CaTiO$_3$:Pr^{3+}@SiO$_2$ photoluminescence materials.

of the other six nitroaromatic explosives and the phosphorescence excitation spectrum of CaTiO$_3$:Pr^{3+}@SiO$_2$, which resulted in poor IFE efficiency (Fig. 4D). On the other hand, we supplemented the FT-IR spectra of CaTiO$_3$:Pr^{3+}@SiO$_2$, TNP, CaTiO$_3$:Pr^{3+}@SiO$_2$ and TNP mixture, respectively, and the results were presented in Fig. S6.† Comparing line b and line c, the band at 1275 cm^{-1} responsible for C–N stretching, at 1155 cm^{-1} for C–O bond stretching, at 1350 cm^{-1} for –NO$_2$ group symmetric stretching and at 1525 cm^{-1} for asymmetric stretching were all hardly shifted, which suggested that there were no chemical bond was formed between CaTiO$_3$:Pr^{3+}@SiO$_2$ and TNP.[42,43] Besides, we also tested the ζ-potential of CaTiO$_3$:Pr^{3+}@SiO$_2$ alone and CaTiO$_3$:Pr^{3+}@SiO$_2$ with NP, DNP and TNP, As showed in Fig. S7,† the average ζ-potential of CaTiO$_3$:Pr^{3+}@SiO$_2$ alone, CaTiO$_3$:Pr^{3+}@SiO$_2$ with NP, DNP and TNP were −22 mV, −23.9 mV, −14.8 mV and −8.29 mV respectively, which meant that the electrostatic interaction between CaTiO$_3$:Pr^{3+}@SiO$_2$ and TNP was higher than that with DNP and NP. As mentioned above, the unprecedented selectivity of CaTiO$_3$:Pr^{3+}@SiO$_2$ toward TNP can be explained by the favorable IFE and electrostatic interactions. Scheme 1 showed the possible mechanism of the phosphorescence quenching detection of TNP based on the CaTiO$_3$:Pr^{3+}@SiO$_2$ photoluminescence materials.

Detection of TNP by CaTiO$_3$:Pr^{3+}@SiO$_2$

According to the above investigation, we found that the phosphorescence intensity decreased with the increasing of TNP, when CaTiO$_3$:Pr^{3+}@SiO$_2$ were free in aqueous solution under UV light off instantaneously, strong red phosphorescence can be observed (Fig. 5A-a). However, in the presence of TNP, the phosphorescence of CaTiO$_3$:Pr^{3+}@SiO$_2$ was quenched significantly (Fig. 5A-b), indicated that CaTiO$_3$:Pr^{3+}@SiO$_2$ possed good TNP response ability. Therefore, in order to exploring the sensing ability of CaTiO$_3$:Pr^{3+}@SiO$_2$ to TNP, phosphorescence quenching titrations were performed with incremental additions of TNP to CaTiO$_3$:Pr^{3+}@SiO$_2$. Fig. 5A showed the quenching of phosphorescence intensity upon the addition of TNP solutions (0–300 μM). The phosphorescence intensity gradually decreased with increasing concentrations of TNP and then reached a plateau when TNP concentration reached 300 μM (Fig. 5B). The maximum phosphorescence intensity of CaTiO$_3$:Pr^{3+}@SiO$_2$ was reduced by when TNP concentration reached 300 μM (Fig. 5B). The maximum phosphorescence intensity of CaTiO$_3$:Pr^{3+}@SiO$_2$ was reduced by 88.2% upon exposure to 300 μM TNP solution. A good linear relationship between phosphorescence signal of (Ip_0/Ip_1) and TNP concentration was observed from 0.5 to 100 μM ($R^2 = 0.998$), with a limit of detection of 20.6 nM. Compared with other systems for ATP detection (Table S1†), our CaTiO$_3$:Pr^{3+}@SiO$_2$ phosphorescence sensor showed lower detection limit and wider linear range.

Determining the concentration of TNP in water samples

To illustrate the feasibility of the phosphorescence TNP sensor in complex matrices, the proposed method was applied in the detection of TNP in pond water samples. The water samples
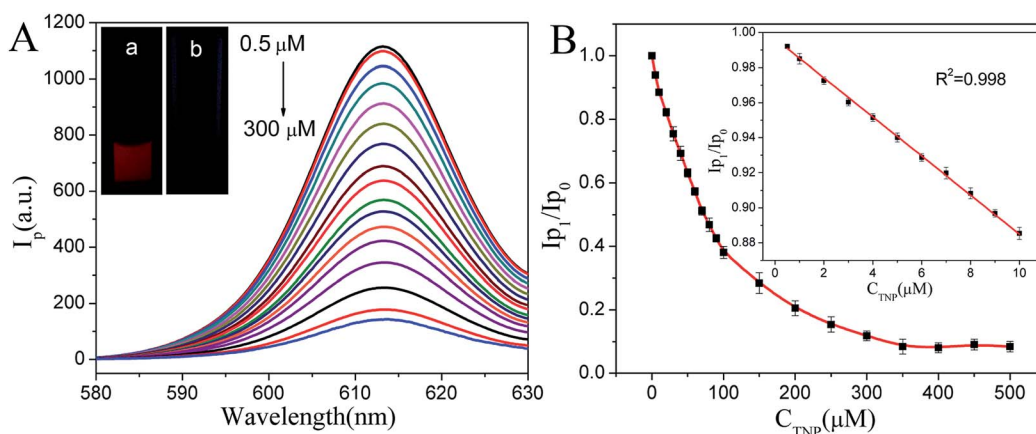

Fig. 5 (A) Phosphorescence spectra of CaTiO$_3$:Pr^{3+}@SiO$_2$ (30 μg mL^{-1}) upon addition of increasing concentrations of TNP (0.5 μM–300 μM) in PBS buffer (pH 8.0, 10 mM). Inset: the photograph of the CaTiO$_3$:Pr^{3+}@SiO$_2$ without (a) and with (b) TNP under UV light off instantaneously. (B) The plot of the value of relative phosphorescence intensities (Ip_0/Ip_1) *versus* the concentration of TNP in PBS buffer (10 mM, pH 8.0). Inset: the linear relationship of relative phosphorescence intensities (Ip_0/Ip_1) *versus* the concentration of TNP over the range from 0.5 μM to 300 μM. Where Ip_1 and Ip_0 were the phosphorescence intensity of CaTiO$_3$:Pr^{3+}@SiO$_2$ with and without TNP. $\lambda_{Ex} = 315$ nm (error bars, SD, $n = 3$).

were transferred to a centrifuge tube and the large particles were separated from the water by centrifugation at 10 000 rpm for 15 min. The reliability and accuracy of the detection method we developed were evaluated through a recovery study, which was carried out on samples spiked with standard TNP solutions (20, 50, 80 μM). The results were satisfactory with the recoveries of 99.34–101.6% (Table S2†), indicating potential applications in the detection of TNP in pond water.

Conclusions

In summary, highly photoluminescent $CaTiO_3:Pr^{3+}@SiO_2$ nanoparticles were synthesized through a solid-state synthesis method, which can act as a sensitive and selective phosphorescent chemosensor for the detection of TNP in aqueous solution without interference from different metal ions, anions and nitroaromatic explosives. As a phosphorescence probe, $CaTiO_3:Pr^{3+}@SiO_2$ has better physical and chemical stabilities, long phosphorescence lifetime and eco-friendliness. The phosphorescence intensity gradually decreased with increasing concentrations of TNP. A good linear relationship between the phosphorescence and TNP concentration was obtained from 0.5 to 100 μM, and the detection limit was as low as 20.6 nM. The IFE and electrostatic interactions were considered to be the main process for the photoluminescence responses for this sensor system. The chemosensor was successfully used to determine the concentration of TNP in water samples, which made it possible for rapid, convenient, sensitive, and selective detection of trace amounts of TNP in environmental and water samples. On conclusion, the developed method is expected to be further applied in environmental pollution analysis.

Conflicts of interest

There are no conflicts to declare.

Acknowledgements

References

1 Y. Peng, A. J. Zhang, M. Dong and Y. W. Wang, *Chem. Commun.*, 2011, **47**, 4505–4507.

2 G. He, H. Peng, T. Liu, M. Yang, Y. Zhang and Y. Fang, *J. Mater. Chem.*, 2009, **19**, 7347–7353.

3 P. Ghosh, S. K. Saha, A. Roychowdhury and P. Banerjee, *Eur. J. Inorg. Chem.*, 2015, **17**, 2851–2857.

4 P. Ghosh and P. Banerjee, *Anal. Chim. Acta*, 2017, **965**, 111–122.

5 M. Dong, Y. W. Wang, A. J. Zhang and Y. Peng, *Chem.–Asian J.*, 2013, **8**, 1321–1330.

6 D. Singha, S. Bhattacharya, P. Majee, S. Mondal, M. Kumar and P. Mahata, *J. Mater. Chem. A*, 2014, **2**, 20908–20915.

7 M. Rong, L. Lin, X. Song, T. Zhao, Y. Zhong, J. Yan, Y. Wang and X. Chen, *Anal. Chem.*, 2015, **87**, 1288–1296.

8 Y. Salinas, R. Martinez-Manez, M. D. Marcos, F. Sancenon, A. M. Costero, M. Parra and S. Gil, *Chem. Soc. Rev.*, 2012, **41**, 1261–1296.

9 M. E. Germain and M. J. Knapp, *Chem. Soc. Rev.*, 2009, **38**, 2543–2555.

10 J. S. Yang and T. M. Swager, *J. Am. Chem. Soc.*, 1998, **120**, 11864–11873.

11 B. Xu, X. Wu, H. Li, H. Tong and L. Wang, *Macromolecules*, 2011, **44**, 5089–5092.

12 Y. Ma, H. Li, S. Peng and L. Wang, *Anal. Chem.*, 2012, **84**, 8415–8421.

13 V. Bhalla, A. Gupta, M. Kumar, D. S. Rao and S. K. Prasad, *ACS Appl. Mater. Interfaces*, 2013, **5**, 672–679.

14 S. Babaee and A. Beiraghi, *Anal. Chim. Acta*, 2010, **662**, 9–13.

15 M. López-López and C. García-Ruiz, *TrAC, Trends Anal. Chem.*, 2014, **54**, 36–44.

16 D. S. Moore, *Rev. Sci. Instrum.*, 2004, **75**, 2499–2512.

17 R. Mu, H. Shi, Y. Yuan, A. Karnjanapiboonwong, J. G. Burken and Y. Ma, *Anal. Chem.*, 2012, **84**, 3427–3432.

18 K. Badjagbo and S. Sauvé, *Crit. Rev. Anal. Chem.*, 2012, **42**, 257–271.

19 J. M. Sylvia, J. A. Janni, J. D. Klein, K. M. Spencer and A. Chem, *Anal. Chem.*, 2000, **72**, 5834–5840.

20 R. Hodyss and J. L. Beauchamp, *Anal. Chem.*, 2005, **77**, 3607–3610.

21 P. Ghosh, S. Paul and P. Banerjee, *CrystEngComm*, 2017, **19**, 6703–6710.

22 P. Ghosh, J. Das, A. Basak, S. K. Mukhopadhyay and P. Banerjee, *Sens. Actuators, B*, 2017, **251**, 985–992.

23 Q. Zhao, C. Huang and F. Li, *Chem. Soc. Rev.*, 2011, **40**, 2508–2524.

24 V. W. Yam and K. M. Wong, *Chem. Commun.*, 2011, **47**, 11579–11592.

25 L. He, J. Qiao, L. Duan, G. Dong, D. Zhang, L. Wang and Y. Qiu, *Adv. Funct. Mater.*, 2009, **19**, 2950–2960.

26 Y. Chi and P. T. Chou, *Chem. Soc. Rev.*, 2010, **39**, 638–655.

27 R. D. Costa, E. Ortí, H. J. Bolink, F. Monti, G. Accorsi and N. Armaroli, *Angew. Chem., Int. Ed.*, 2012, **51**, 8178–8211.

28 P. T. Diallo, P. Boutinaud, R. Mahiou and J. C. Cousseins, *Phys. Status Solidi A*, 2015, **160**, 255–263.

29 Z. Pan, Y. Y. Lu and F. Liu, *Nat. Mater.*, 2012, **11**, 58–63.

30 W. Zeng, Y. Wang, S. Han, W. Chen, G. Li, Y. Wang and Y. Wen, *J. Mater. Chem. C*, 2013, **1**, 3004–3011.

31 Y. Luo and Z. Xia, *J. Phys. Chem. C*, 2014, **118**, 23297–23305.

32 R. Ali and M. Yashima, *J. Solid State Chem.*, 2005, **178**, 2867–2872.

33 H. J. A. Koopmans, G. M. H. V. D. Velde and P. J. Gellings, *Acta Crystallogr., Sect. C: Cryst. Struct. Commun.*, 1983, **39**, 1323–1325.

34 P. Boutinaud, L. Sarakha, E. Cavalli, M. Bettinelli, P. Dorenbos and R. Mahiou, *J. Phys. D: Appl. Phys.*, 2009, **42**, 45106–45112.

35 Y. Inaguma, T. Muronoi, K. Sano, T. Tsuchiya, Y. Mori, T. Katsumata and D. Mori, *Inorg. Chem.*, 2011, **50**, 5389–5395.

36 B. Wang, H. Lin, J. Xu, H. Chen, Z. Lin, F. Huang and Y. Wang, *Inorg. Chem.*, 2015, **54**, 11299–11306.

37 X. Zhang, J. Zhang, X. Ren and X. J. Wang, *J. Solid State Chem.*, 2008, **181**, 393–398.

38 X. Zhang, J. Zhang, X. Zhang, M. Wang, H. Zhao, S. Lu and X. Wang, *J. Phys. Chem. C*, 2007, **111**, 18044–18048.

39 K. Sue, S. Kawasaki, T. Sato, D. Nishiohamane, Y. Hakuta and T. Furuya, *Ind. Eng. Chem. Res.*, 2016, **55**, 7628–7634.

40 R. Chen and D. Chen, *Spectrochim. Acta, Part A*, 2014, **127**, 256–260.

41 Y. Wang and Y. Ni, *Anal. Chem.*, 2014, **86**, 7463–7470.

42 P. Ghosh and P. Banerjee, *Phys. Chem. Chem. Phys.*, 2016, **18**, 22805–22815.

43 P. Ghosh, P. Roy, A. Ghosh, S. Jana, N. C. Murmu, S. K. Mukhopadhyay and P. Banerjee, *J. Lumin.*, 2017, **185**, 272–278.